Phase Dependent Vectorial Current Control in Symmetric Noisy Optical Ratchets

Magda G. Sánchez-Sánchez, Roberto de J. León-Montiel,* and Pedro A. Quinto-Su†
Instituto de Ciencias Nucleares, Universidad Nacional Autónoma de México, Apartado Postal 70-543, 04510 Cd. Mx., México

(Received 4 March 2019; revised manuscript received 21 August 2019; published 22 October 2019)

In this work, we demonstrate single microparticle transport in a symmetric noisy optical ratchet made with a linear array of 20 optical potentials, where each potential is a spatially symmetric low power (< 2.5 mW) three-dimensional trap. Both the external force $F(t)$ and the depth $V_{0i}(t)$ of the optical potentials are dynamic and change at the same frequency $\nu = 2$ Hz. The depths of the individual optical potentials are random (uncorrelated noise) distributed around a mean value V_0, $\langle V_{0i}(t)\rangle = V_0$, while the external force is periodic and unbiased $\langle F(t)\rangle = 0$. The system is completely symmetric for times $t \gg 1/\nu$. Directed transport is possible as a result of the symmetry being broken at times on the order of $1/\nu$. We find that the direction and speed of motion (current) are coupled to the phase difference between the noise in the optical potentials and the external periodic force.

DOI: 10.1103/PhysRevLett.123.170601

Transport phenomena are ubiquitous to a wide variety of disciplines ranging from biology, chemistry, physics, and even electronics [1–9]. In particular, directed motion of particles has become a major research topic [10], mainly because of its fundamental role in understanding the functioning of natural systems, such as the movement of motor proteins along tubulin molecules [11–13], which has lead to novel applications ranging from microparticle sorting [14], to the directed motion of cold [15,16] and ultracold atoms [17], to the control of electronic transport through semiconductor superlattices [18].

Interestingly, unidirectional motion in the micro- and nanoscale has been achieved by means of ratchet systems, where the movement of a particle is mediated by a fine-tuned combination of a zero-average periodic external force and asymmetric potentials which privilege motion in one direction while hindering it in the opposite [19–27]. In general, directed transport is achieved by introducing an asymmetry (for example, in the spatial shape of the potentials). Hence, if the asymmetric potentials in the previous studies were changed to symmetric potentials, directed transport would be destroyed [28], and new approaches would have to be considered [29,30]. Among these, the simplest strategy consists of introducing a nonzero, constant, strong tilting force to the potentials, which drives the system out of equilibrium, thus producing movement of the particle [31]. Another approach is to use a weak tilting force—smaller than the one necessary to make the particle escape the potentials—in combination with dynamically disordered potentials [32]. Finally, the third and most difficult way of producing directed motion is by incorporating correlated noise, rather than white or Brownian, to the dynamics of the particle [33].

In this work, we show numerically and experimentally that directed motion of a single particle can be observed in a dynamical system with a characteristic frequency ν made of a linear array of Gaussian potentials and a periodic external force. In particular, the time averages $\langle \ldots \rangle$ of the external force and the potential array result in a completely symmetric system for times that are much longer than the inverse of the frequency. The system is robust and can be implemented using the simplest methods of holographic optical tweezers.

The main components of the symmetric noisy ratchet are as follows: (1) A linear array of N focused laser beams that create the optical potentials [Fig. 1(a)] which can be modeled with Gaussian potentials [34,35]

$$V(x,t) = -\sum_{i=1}^{N} V_{0i}(t) \exp\left(-\frac{(x-iL)^2}{2\sigma^2}\right), \qquad (1)$$

where σ is the spot size and L the interpotential separation [Fig. 1(a)]. The depths of the potentials are random $V_{0i}(t) = V_0 + \phi_i(t)$, where $\phi_i(t)$ are uncorrelated random Gaussian stochastic variables with $\langle \phi_i(t)\rangle = 0$ so that $\langle V_{0i}(t)\rangle = V_0$ [Fig. 1(b)]. The standard deviation of the noise $\phi_i(t)$ is set to $0.23V_0$ to match the experiment. The N potentials are updated simultaneously at the same frequency ν as an external force [Fig. 1(c), red dotted line for one potential]. Hence the potentials are static during a time $\tau = 1/\nu$. (2) An external unbiased periodic force $\langle F(t)\rangle = 0$. $F(t) = F_d\Omega(2\pi\nu t + \tilde{\phi})$, where $\Omega(t)$ describes a zero-average periodic function, with a frequency ν and a $\tilde{\phi}$ phase shift. Here, $F(t)$ is a square wave so that the force is constant and changes sign at half the period [Fig. 1(c)].

The phase difference $\Delta\phi$ is the difference between $\tilde{\phi}$ and the initial phase of the potentials which here is set to zero. The mean depth in the potentials V_0 is sufficiently large to

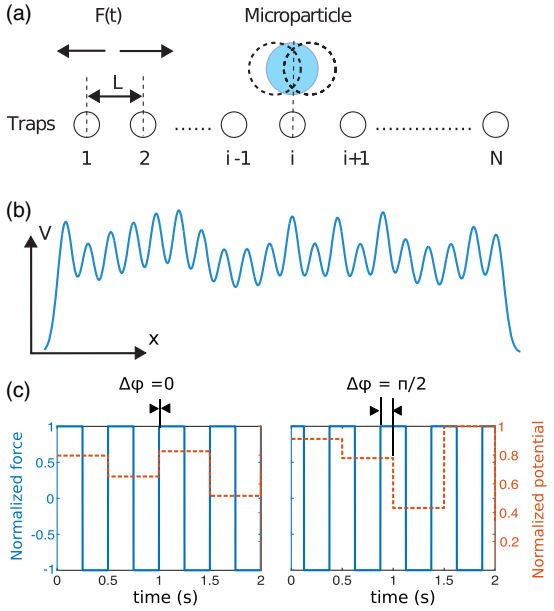

FIG. 1. (a) Sketch of the system showing the position of the optical traps (separated by $L = 2.3$ μm, $\sigma = 519$ nm) and the position of a particle (blue circle) trapped by the ith trap. Once the external rocking force $F(t)$ is introduced, the trapped particle will oscillate around the ith trap (dotted circles). (b) Linear optical potential array with random heights $V_{0i}(t_0)$. (c) Dynamics of the experiment: The external force is represented by the blue line (constant during half-period), and the red line represents the change into one of the optical potentials; the first plot is the case for zero phase difference and the second plot is for a phase difference of $\pi/2$.

hold a microparticle in a trap even under the action of $F(t)$. In this way, there is no transport with static potentials.

The system is completely symmetric for times $t \gg \tau$ ($\langle F(t)\rangle = 0$ and $\langle V_{0i}(t)\rangle = V_0$), so the only way to get directed transport is to use the random spatial asymmetry in the depths of the potentials during the time τ where the potentials are static.

Figure 1(a) shows the way directed transport is achieved: Assuming that the particle (blue circle) is trapped by the ith potential, the particle is periodically displaced (dotted circles) by the external force while the depths of the potentials are changed during a time interval τ [the exact time defines the phase difference $\Delta\phi$ as shown in Fig. 1(c)]. If the potentials are updated at a time when the particle is at the largest separation from its trapping potential, either between i and $i+1$ or between i and $i-1$, then it is possible that the random change in the depths of the potentials could pull the particle to $i+1$ or $i-1$ (depending on the relative strength of the potentials). This shows that the relative phase between the force and the noise [Figs. 1(a) and 1(c)] in the potentials controls transport direction and speed.

To describe the dynamics of the system, we consider the motion of a Brownian particle under the external periodic force $F(t)$ and the linear array of optical potentials $V(x,t)$ described previously. The Langevin equation for the particle in the overdamped limit [36] is

$$\dot{x} = -\frac{1}{\gamma}[V'(x,t) + F(t)] + \sqrt{2k_BT/\gamma}\xi(t). \qquad (2)$$

Here, γ characterizes the friction of the particle immersed in liquid, and $\sqrt{2k_BT/\gamma}\xi(t)$ the thermal noise due to random collisions with the surrounding fluid molecules. $\xi(t)$ stands for a Gaussian Markov stochastic process with zero average and unit-delta autocorrelation function, k_B is the Boltzmann constant, and T the temperature of the system.

The solution of Eq. (2) explicitly depends on the values that the stochastic Gaussian variables $\phi_i(t)$ (noise in the depths of the potentials) and $\xi(t)$ (Brownian) take during the evolution of the system. Hence, the system is solved numerically with the parameters of the experiment. Details are in Secs. 1 and 2 of the Supplemental Material [37], which includes Refs. [38,39].

The experiment explores the dynamics of a single microparticle trapped in a linear array of $N = 20$ optical potentials with an interpotential separation $L = 2.3 \pm 0.1$ μm. The microparticle sample is composed of silica microbeads with a mean diameter $2R$ of 2.47 μm immersed in water. The external force is realized by dragging the microscope stage at a constant speed to get a constant force ($F_d = 6\pi\eta R v$; see Supplemental Material [37], Sec. 3) at a frequency $\nu = 2$ Hz.

The linear array of optical potentials are created by shaping the trapping laser beam with a spatial light modulator (SLM). This is done by changing the projected digital holograms at the same rate ν as the external force, simultaneously updating the 20 traps. The digital holograms are calculated with the simple Gershberg-Saxton algorithm [40], randomly changing the target intensity at the potentials, the depth $V_{0i}(t)$. The variation in the diffracted power to the individual traps has a standard deviation of $\pm 23\%$. The mean diffracted power into all of the traps is 37 mW (transmitted by the microscope objective). In the case of one realization, the total power is proportional to $\sum_i V_{0i} = NV_0 + \sum_i \phi_i$, showing that there are variations around the mean value. In the experiment, these variations also appear during individual realizations on the total diffracted power. However, the average power is constant. The mean power per trap (1.85 mW) is proportional to the mean potential depth $V_0 = 6.4 \times 10^{-19}$ J ~ 155 k_BT ($T = 300$ K) fitted from the dynamics of the experiment. The measured escape velocity for different projected patterns is 49.4 ± 17.8 μm/s.

Here, it is worth mentioning that in contrast with the model, where the changes in the force and the potentials are instantaneous [Fig. 1(c)], in the experiment each time the hologram is changed there is flickering, which results in a lowering of a diffracted power to the trap. In our

experiment, we found that during a hologram-switching event the particle is essentially free for about 5 ms; this results in a displacement of 119 nm, which is a very small fraction (4%) of the interpotential separation L. Furthermore, the experimental results are reasonably reproduced by the numerical model.

Figure 2(a) is the experimental analog of Fig. 1(c), and it shows the displacement of the piezo stage (reference microparticle) and the changes in the optical potentials. The displacement speed of the stage is constant, so that the force is constant over half a cycle like in the case of the model [Fig. 1(c)]. The red line indicates when the SLM is updated (see the Supplemental Material [37], Sec. 3, Fig. 3), and this signal is obtained from a speckle pattern that is projected into the camera. In the case of the external force, we observe that the slope (speed) depends on the amplitude of the stage motion. In this case, the amplitude is $6.1 \pm 0.3\ \mu$m and the speed is $23.8 \pm 1.6\ \mu$m/s. Figure 2(b) shows the displacement of the trapped particle for a single phase difference of 1.1 rad in 37 cycles (black lines) and the average displacement (red line). Notice that after averaging over all the trajectories (red line), the particle does not return to its initial position but a finite, small distance above it. This phase-controlled movement within one cycle is what we define as the mean displacement per cycle.

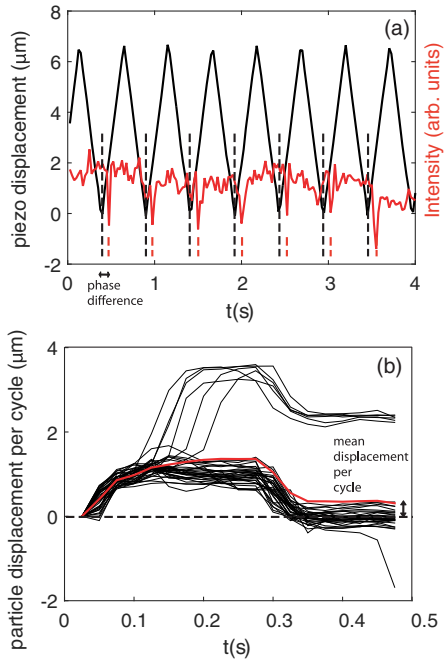

FIG. 2. (a) Measured trajectory of a reference microparticle stuck at the bottom of the microscope coverslip. The red line is part of a speckle pattern that is used to track the update in the SLM (dips). The phase difference is 1.1 rad. (b) Measured trajectories of the trapped microparticle for each cycle. The red line represents the average trajectory over 37 different realizations for a phase difference of 1.1 rad.

To find the relation between phase and mean displacement, the experiment is performed in the following way: A particle is trapped by one of the potentials and raised to a height of 12 μm. Then, the video of digital holograms is projected (2 Hz) into the SLM, and we confirm that in the absence of external force there is no transport (see Supplemental Material [37], Fig. 4). The next step is to pause the SLM and introduce the external force (2 Hz) of the microscope stage to check that there is no transport with static potentials either (see Supplemental Material [37], Fig. 4). The transport experiment is then started with both the SLM video and the periodic external force. The phase difference between both signals is controlled by varying the phase of the external force that is controlled by a function generator (triangular wave). This is done by changing the phase in the output of the instrument which is computer controlled. The phase in the function generator is changed in steps of 40 deg (~0.70 rad). In order to avoid the particle reaching one of the boundaries (initial and last traps), each

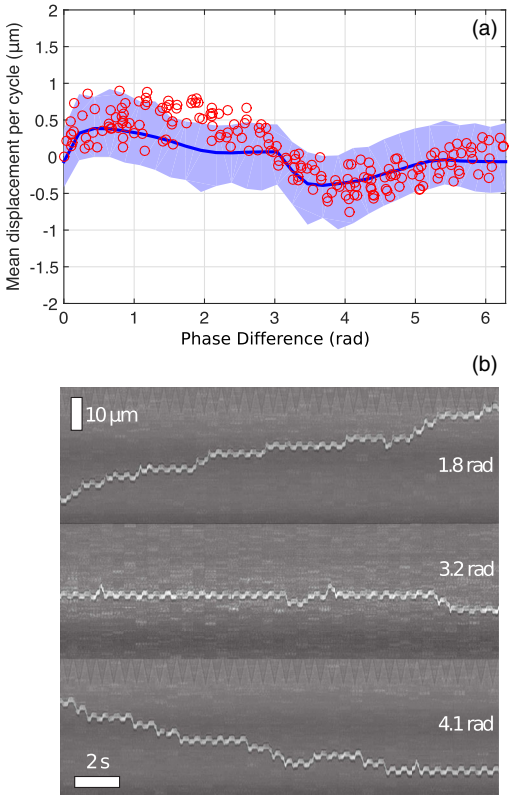

FIG. 3. (a) Average displacement (per cycle) of the particle as a function of the periodic-force phase ϕ. The red round markers correspond to 37 different realizations of the experiment. The blue shaded region is composed of 1000 independent numerical realizations of the experiment, showing that the measured signals are expected within our simplified model. (b) Composite images for phase differences of 1.8, 3.2, and 4.1 rad for a time of 19.5 s. Each video frame is cut to a width of three pixels and each composite image contains 780 frames. The video in the Supplemental Material shows the case of negative displacement (to the left).

phase is switched every 20 s by πrad. In this way, we start with zero rad at the output of the function generator, followed by $\pi, 0.7, 0.7+\pi, \ldots$.

The results of our experiments are depicted in Fig. 3. The average displacement per cycle as a function of phase difference is plotted in Fig. 3(a). Each data point represents the average over 37 cycles. The blue solid line corresponds to the average displacement of the particle obtained by numerically solving Eq. (2) with the parameters of our experiment. Our simulations are performed by making use of a simple finite difference algorithm (see Ref. [36] and the Supplemental Material [37]). The shaded region of Fig. 3(a) shows 1000 independent numerical realizations of the experimental procedure described above, with the solid line depicting the average of the realizations. Note that the average displacement shows an important symmetry over the phase difference; in particular, for a phase difference between 0 and π, the movement of the particle follows a positive direction, whereas for a phase difference between π and 2π, the movement goes in the opposite direction. Note that the experimental results are well captured by our simplified model, showing that the particle's motion can indeed be controlled by properly setting the phase difference between the drag and noise signals. The experimental data are not completely symmetric, transport is slightly faster in the range between 0 and π, which could be a result of a small asymmetry in the external force.

Figure 3(b) shows three different trajectories (positive, neutral, and negative displacements) extracted from videos with phase differences of 1.8, 3.2, and 4.1 rad. The images are composed of slices with a width of three pixels for each video frame. The particle center appears bright, so that the trajectory for more than 19 s looks like a white line in the composite image. The video in the Supplemental Material shows a case with negative displacement (movement to the left).

Comparing our results with most ratchet systems [20,21,24], our implementation offers a relatively simple way of controlling direction and speed. This system is also quite robust as the potentials are calculated with one of the simplest methods [40] without requiring high uniformity. Another useful property of this ratchet is that the traps are 3D, which is not a property of all optical ratchet systems. Other theoretical studies have proposed current reversals based on gated ratchets controlled by the phases of two harmonic signals [41].

In conclusion, we have presented a phase-controlled symmetric ($\langle V_{0i}(t)\rangle = V_0$, $\langle F(t)\rangle = 0$) noise-enabled optical ratchet where the magnitude and direction of the current can be adjusted by changing the phase difference between noise and external force. Contrary to conventional knowledge, our results demonstrate that particle motion in symmetric potentials subjected to a periodic zero-average external force can be observed and manipulated by introducing simple Gaussian white noise to the potentials. More importantly, we have shown that the direction of the particle's motion can easily be controlled by changing the relative phase between the force and noise signals. This might help expand the scope of particle transport in symmetric potentials and open the door to new noise-enabled micro- and nanoscale applications.

Because of its simplicity and versatility, our experiment constitutes a robust platform for the study of directed motion across symmetric potentials and paves the way toward the development of novel noise-enabled micro- and nanoscale transport technologies.

The work was partially funded by the following grants: DGAPA-UNAM Grants No. PAPIIT IA100718 and No. IN107719 and Conacyt Grants No. CB-2016-01/284372, No. CB253706, and No. LN293471. P. A. Q. S. thanks Mr. José Rangel Gutiérrez for machining custom optomechanical components.

*roberto.leon@nucleares.unam.mx
†pedro.quinto@nucleares.unam.mx

[1] P. Rebentrost, M. Mohseni, I. Kassal, S. Lloyd, and A. Aspuru-Guzik, New J. Phys. **11**, 033003 (2009).
[2] F. Caruso, A. W. Chin, A. Datta, S. F. Huelfa, and M. B. Plenio, J. Chem. Phys. **131**, 105106 (2009).
[3] R. de J. León-Montiel and J. P. Torres, Phys. Rev. Lett. **110**, 218101 (2013).
[4] J. Spiechowicz, P. Hänggi, and J. Luczka, Phys. Rev. E **90**, 032104 (2014).
[5] R. de J. León-Montiel, I. Kassal, and J. P. Torres, J. Phys. Chem. B **118**, 10588 (2014).
[6] J. Spiechowicz and J. Luczka, Phys. Scr. **T165**, 014015 (2015).
[7] R. de J. León-Montiel, M. A. Quiroz-Juárez, R. Quintero-Torres, J. L. Domínguez-Juárez, H. M. Moya-Cessa, J. P. Torres, and J. L. Aragón, Sci. Rep. **5**, 17339 (2015).
[8] D. N. Biggerstaff, R. Heilmann, A. A. Zecevik, M. Gräfe, M. A. Broome, A. Fedrizzi, S. Nolte, A. Szameit, A. G. White, and I. Kassal, Nat. Commun. **7**, 11282 (2016).
[9] J. Spiechowicz, J. Luczka, and P. Hänggi, Sci. Rep. **6**, 30948 (2016).
[10] P. Hänggi and F. Marchesoni, Rev. Mod. Phys. **81**, 387 (2009).
[11] A. Ajdari and J. Prost, Proc. Natl. Acad. Sci. U.S.A. **88**, 4468 (1991).
[12] S. M. Simon, C. S. Peskin, and G. F. Oster, Proc. Natl. Acad. Sci. U.S.A. **89**, 3770 (1992).
[13] S. Leibler, Nature (London) **370**, 412 (1994).
[14] L. R. Huang, E. C. Cox, R. H. Austin, and J. C. Sturm, Science **304**, 987 (2004).
[15] R. Gommers, S. Denisov, and F. Renzoni, Phys. Rev. Lett. **96**, 240604 (2006).
[16] R. Gommers, V. Lebedev, M. Brown, and F. Renzoni, Phys. Rev. Lett. **100**, 040603 (2008).
[17] T. Salger, S. Kling, T. Heckling, C. Geckeler, L. Morales-Molina, and M. Weitz, Science **326**, 1241 (2009).
[18] F. G. Bass and A. Bulgakov, *Kinetic and Electrodynamic Phenomena in Classical and Quantum Semiconductor*

Superlattices (Nova Science Publishing, Commack, NY, 1997).
[19] L. P. Faucheux, L. S. Bourdieu, P. D. Kaplan, and A. J. Libchaber, Phys. Rev. Lett. **74**, 1504 (1995).
[20] S.-H. Lee, K. Ladavac, M. Polin, and D. G. Grier, Phys. Rev. Lett. **94**, 110601 (2005).
[21] A. V. Arzola, K. Volke-Sepúlveda, and J. L. Mateos, Phys. Rev. Lett. **106**, 168104 (2011).
[22] Y. Hasegawa and M. Arita, J. R. Soc. Interface **9**, 3554 (2012).
[23] P. A. Huidobro, S. Ota, X. Yang, X. Yin, F. J. García-Vidal, and X. Zhang, Phys. Rev. B **88**, 201401(R) (2013).
[24] A. V. Arzola, M. Villasante-Barahona, K. Volke-Sepulveda, P. Jakl, and P. Zemanek, Phys. Rev. Lett. **118**, 138002 (2017).
[25] M. von Smoluchowski, Phys. Z. **13**, 1069 (1912).
[26] R. P. Feynman, *The Feynman Lectures on Physics* (Addison-Wesley, Reading, MA, 1963), Vol. 1.
[27] P. Hänggi and R. Bartussek, Lect. Notes Phys. **476**, 294 (1996).
[28] P. Reimann, Phys. Rev. Lett. **86**, 4992 (2001).
[29] S. Flach, O. Yevtushenko, and Y. Zolotaryuk, Phys. Rev. Lett. **84**, 2358 (2000).
[30] Z. Zheng, G. Hu, and B. Hu, Phys. Rev. Lett. **86**, 2273 (2001).
[31] P. Reimann, Phys. Rep. **361**, 57 (2002).
[32] R. de J. León-Montiel and P. A. Quinto-Su, Sci. Rep. **7**, 44287 (2017).
[33] J. Łuczka, R. Bartussek, and P. Hänggi, Europhys. Lett. **31**, 431 (1995).
[34] S.-H. Lee and D. Grier, J. Phys. Condens. Matter **17**, S3685 (2005).
[35] M. Pelton, K. Ladavac, and D. G. Grier, Phys. Rev. E **70**, 031108 (2004).
[36] G. Volpe and G. Volpe, Am. J. Phys. **81**, 224 (2013).
[37] See Supplemental Material at http://link.aps.org/supplemental/10.1103/PhysRevLett.123.170601 for a detailed description of the experimental and numerical methods used in this study, which includes Refs. [38,39].
[38] R. de J. León-Montiel, J. Svozilik, and J. P. Torres, Phys. Rev. E **90**, 012108 (2014).
[39] J. Leach, H. Mushfique, S. Keen, R. Di Leonardo, G. Ruocco, J. M. Cooper, and M. J. Padgett, Phys. Rev. E **79**, 026301 (2009).
[40] R. W. Gerchberg and W. O. Saxton, Optik (Stuttgart) **35**, 237 (1972).
[41] L. Dinis and N. R. Quintero, Phys. Rev. E **91**, 032920 (2015).